AIP | Applied Physics Letters

Opto-electrical properties of Sb-doped p-type ZnO nanowires

Tzu-Hsuan Kao, Jui-Yuan Chen, Chung-Hua Chiu, Chun-Wei Huang, and Wen-Wei Wu

Citation: Applied Physics Letters **104**, 111909 (2014); doi: 10.1063/1.4869355
View online: http://dx.doi.org/10.1063/1.4869355
View Table of Contents: http://scitation.aip.org/content/aip/journal/apl/104/11?ver=pdfcov
Published by the AIP Publishing

Opto-electrical properties of Sb-doped p-type ZnO nanowires

Tzu-Hsuan Kao,[a] Jui-Yuan Chen,[a] Chung-Hua Chiu, Chun-Wei Huang, and Wen-Wei Wu[b]
Department of Materials Science and Engineering, National Chiao Tung University, Hsinchu, Taiwan

(Received 18 December 2013; accepted 11 March 2014; published online 20 March 2014)

P-type ZnO nanowires (NWs) have attracted much attention in the past years due to the potential applications for optoelectronics and piezotronics. In this study, we have synthesized Sb-doped p-type ZnO NWs on Si (100) substrates by chemical vapor deposition with Aucatalyst. The Sb-doped ZnO NWs are single crystalline with high density, grown along [1-1-2] direction. The doping percentage of Sb is about 2.49%, which has been confirmed by X-ray photoelectron spectroscopy. The ZnO NW field effect transistor demonstrated its p-type characteristics. A high responsivity to ultraviolet photodetection was also observed. In addition, compared to intrinsic ZnO NWs, the conductivity of the Sb-doped ZnO NWs exhibited ~2 orders of magnitude higher. These properties make the p-type ZnO NWs a promising candidate for electronic and optoelectronic devices. © *2014 AIP Publishing LLC*. [http://dx.doi.org/10.1063/1.4869355]

A wide range of ZnO nanostructures, such as nanowires, nanobelts, nanocombs, nanorods, nanohelixes, and nanotubes, have been synthesized through different growth methods.[1] ZnO nanostructures have attracted great attention due to its wide band gap (3.37 eV) and large exciton binding energy (60 meV). These characteristic features make ZnO a promising material for piezoelectronic and optoelectronic devices, such as nanosensors,[2–4] dye-sensitized solar cells,[5] field effect transistors (FETs),[6] light-emitting diodes,[7,8] and nanogenerators.[9,10] In order to extend the application possibility of ZnO-based devices, several doping elements have been studied and reported, such as Ga, N, In, and Sn.[11–14] However, it is difficult to achieve p-type doping in ZnO. Recently, there were reports indicating that doping with group V elements, such as phosphorous (P),[15] arsenic (As),[16] and antimony (Sb),[17] was achieved, and the p-type materials exhibited superior electrical properties. Among the group V elements, antimony has similar ionic radius to that of Zn ion.[18] Some reports suggested that doping with antimony might produce more stable p-type conductivity and higher carrier concentration.[19,20] To date, Sb-doped ZnO nanostructures can be synthesized by different methods including vapor phase transport,[21,22] hydrothermal method,[23] pulse-laser ablation,[24] and metal-organic chemical vapor deposition (MOCVD).[25] Therefore, Sb-doped ZnO is deemed as a candidate material to achieve p-type properties.

In this work, we report the growth of Sb-doped p-type ZnO nanowires (NWs) on Si substrate by thermal evaporation method via the vapor-liquid-solid (VLS) mechanism. The Sb doping concentration was also measured. Photoluminescence (PL) results revealed the Sb-doped ZnO NWs possess high concentrations of impurities and the non-band-edge emission peak presented red-shifted as compared to pure ZnO NWs. P-type transport property was confirmed by single NW-based FETs. Furthermore, theSb-doped ZnO NW UV photodetector shows a remarkable photoresponse with high on/off ratio.

Sb-doped ZnO NWs were synthesized on (100) Si substrates. Zinc and Antimony powders were mixed with a weight ratio of 5:2 as precursors in an aluminum boat. The boat was placed in the center of a horizontal three-zone furnace. The mixed-source was placed at upstream and the Si substrate was placed at downstream, respectively. The flow rates of Ar and O_2 gases were 60 sccm and 5 sccm, respectively, while the chamber pressure was held at 3 Torr. The temperature of the furnace was raised to 650 °C with a heating rate of 10 °C/min and maintained for 30 min. After the growth process, the test samples were fabricated by photolithography, e-beam lithography, and e-gun deposition processes.

The morphology and structure of Sb-doped ZnO NWs were characterized by field-emission scanning electron microscope (FESEM, JEOL JSM-6500), X-ray diffractometer (XRD, Bruker D2 phaser), and spherical aberration corrected scanning transmission electron microscope (Cs-corrected STEM, JEOL ARM200F). The chemical analysis of Sb-doped ZnO NWs was conducted by high resolution X-ray photoelectron spectroscopy (XPS) (ULVAC-PHI AES-650). Room temperature PL spectroscope with He-Cd (325 nm) laser was used to investigate the optical properties of Sb-doped ZnO NWs. The NW-FET was fabricated by standard photolithography with a 200-nm-thicksilicon oxide substrate. Sb-doped ZnO NWs were dispersed on the patterned silicon substrate, following by e-beam lithography to define the pattern of the electrode. All the electrodes were deposited by E-gun evaporator (Ni (30 nm)/Au (120 nm)).The electrical properties of the NW-FETs were measured by a semiconductor parameter analyzer (Agilent B1500A). The photoresponse properties of Sb-doped ZnO NWs based photodetectors were examined with a 4 W UV lamp. The opto-electrical properties were all conducted in ambient condition at room temperature.

Fig. 1(a) shows the FESEM image of as-synthesized Sb-doped ZnO NWs. The NWs exhibit a high aspect ratio with the length up to 10–20 μm and diameter ~90 nm. The effects of growth parameters were systematically studied (see supplementary material,[37] Figs. S1–S3). The structure of Sb-doped ZnO NWs was confirmed by the XRD pattern, as shown in Fig. 1(b).The XRD pattern indicated that the peaks corresponded to (100), (002), (101), (102), and (110) planes

[a]T.-H. Kao and J.-Y. Chen contributed equally to this work.
[b]Author to whom correspondence should be addressed. Electronic mail: WWWu@mail.nctu.edu.tw

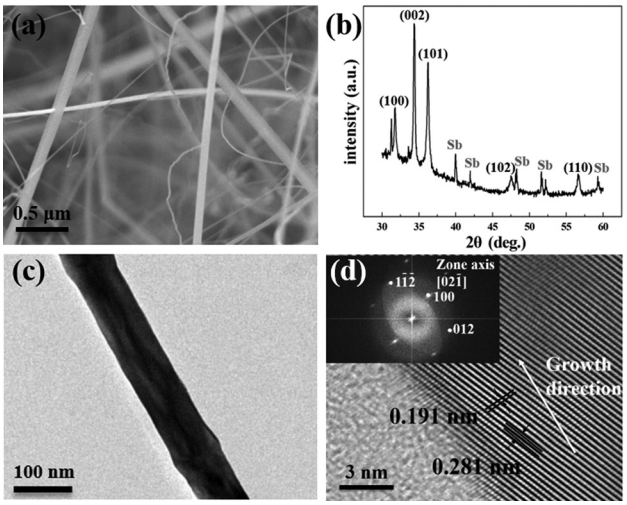

FIG. 1. (a) FESEM image of Sb-doped ZnO NWs; (b) XRD pattern of as-synthesized sample; (c) low magnification image; and (d) HRTEM image of Sb-doped ZnO NWs. The inset shows the corresponding FFT diffraction pattern.

of ZnO wurtzite structure. However, some remaining peaks are denoted as Sb. We inferred that the peaks corresponded with Sb were attributed to the crystalline Sb particle on the Si substrate surface. Figs. 1(c) and 1(d) show the low magnification and HRTEM image of the Sb-doped ZnO NW. The inset in (d) is the corresponding faster Fourier transformation (FFT) diffraction pattern with [02-1] zone axis, indicating the growth direction of the NW is [1-1-2] direction. The interplanar spacing was calculated to be 0.19 nm and 0.28 nm, corresponding to the planes of (1-1-2) and (100), respectively.

Fig. 2(a) shows the TEM energy dispersive spectroscopy (EDX) mapping of the Sb-doped ZnO NW. With the visualized elemental distribution of zinc, oxygen, and antimony, it indicated that Sb was doped uniformly into ZnO NW. XPS spectra of Sb-doped ZnO NWs and pure ZnO NWs were shown in Fig. 2(b), analyzing the chemical bonding and Sb concentration of the doped ZnO NWs. The pure ZnO NWs possess a O-1 S peak at 530.6 eV, whereas the as-synthesized Sb-doped ZnO NWs contained an additional peak at 539.4 eV, corresponding to Sb-3d^3, and a stronger peak at 530.6 eV, attributing to Sb-3d^5.[26,27] Through the quantitative of XPS spectrum, the Sb concentration in doped ZnO NWs is about 2.49 at%.

Fig. 3(a) shows the room temperature PL spectra of Sb-doped ZnO NWs and pure ZnO NWs, while Fig. 3(b) is the spectrum highlighted in (a). PL spectra of pure ZnO NWs possess a strong UV emission peak at 3.369 eV, corresponding to the near band edge emission (NBE). The NBE peak is responsible for the free exciton recombination of ZnO. After doping with Sb, the NBE peak had red-shifted to 3.315 eV and broadened prominently.[28] It is remarkable that there is another peak near the NBE peak in both pure and Sb doped ZnO. The investigation about the NBE of ZnO has been reported, which indicates the peak at ~3.332 eV is due to structure defects.[29] Therefore, the two peaks in pure ZnO (the black line in Fig. 3(b)) can be explained that the peak at 3.369 eV is due to the recombination of free excitons and peak at 3.324 eV is due to the structure defects. Furthermore, the peak at 3.362 eV in Sb-

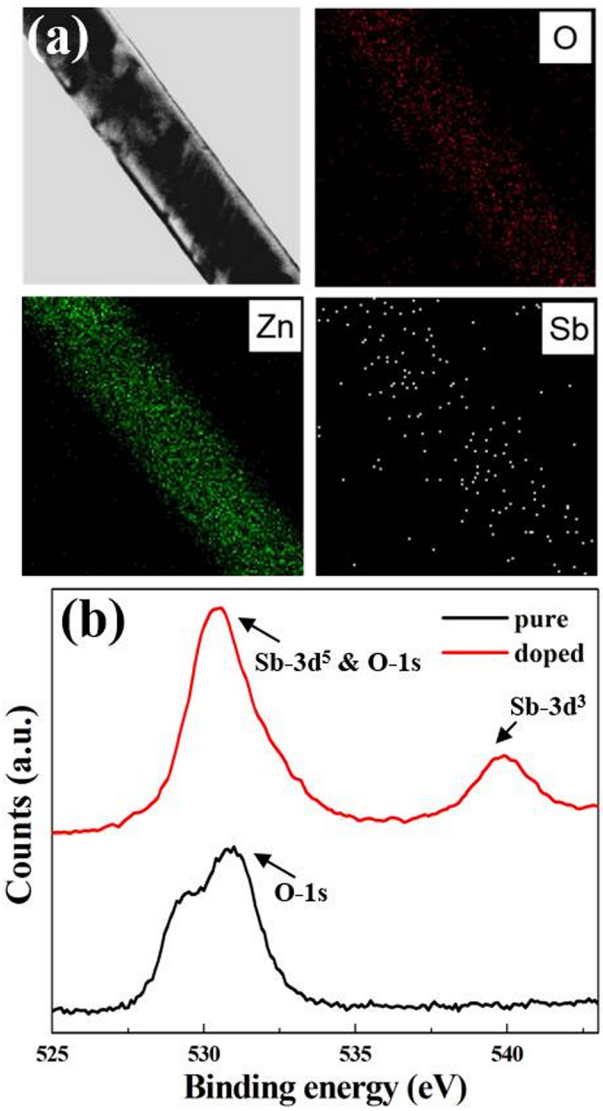

FIG. 2. (a) The TEM EDX mapping of Sb-doped ZnO NWs. (b) XPS spectrum of Sb-doped ZnO NWs and pure ZnO NWs.

doped ZnO attribute to the structure defects. Therefore, the red-shift effect in the peak, which is contributing to the recombination of free excitons, shift from 3.369 eV to 3.315 eV. This result confirmed the red-shift effect by Sb doping. Previous reports indicated that the broadening of the NBE peak is due to band tailing in the gap as well as the introduction of an impurity into the semiconductor materials.[30] In addition, we investigate that it possesses a strong green emission of as-synthesized sample in contrast to pure ZnO NWs. This is deemed as the incorporation of doping species on the valence band.[31,32] Fig. 3(c) shows the temperature-dependent PL of Sb-doped ZnO NWs from 10 to 280 K. The intensity of NBE peak decrease with increasing temperature as expected due to thermal vibration.[33,34]

The electrical properties and p-type conductivity of the Sb-doped ZnO NWs were confirmed by the single NW-FET on the n^+-silicon substrate as the back gate electrode. Fig. 4(a) shows the schematic diagram of the NW-FET device and the fabrication processes were in supplementary material, Fig. S4.[37] Figs. 4(b) and 4(c) show the drain current (I_d) vs voltage (V_d) curve at various gate voltage (V_g) and I_d vs

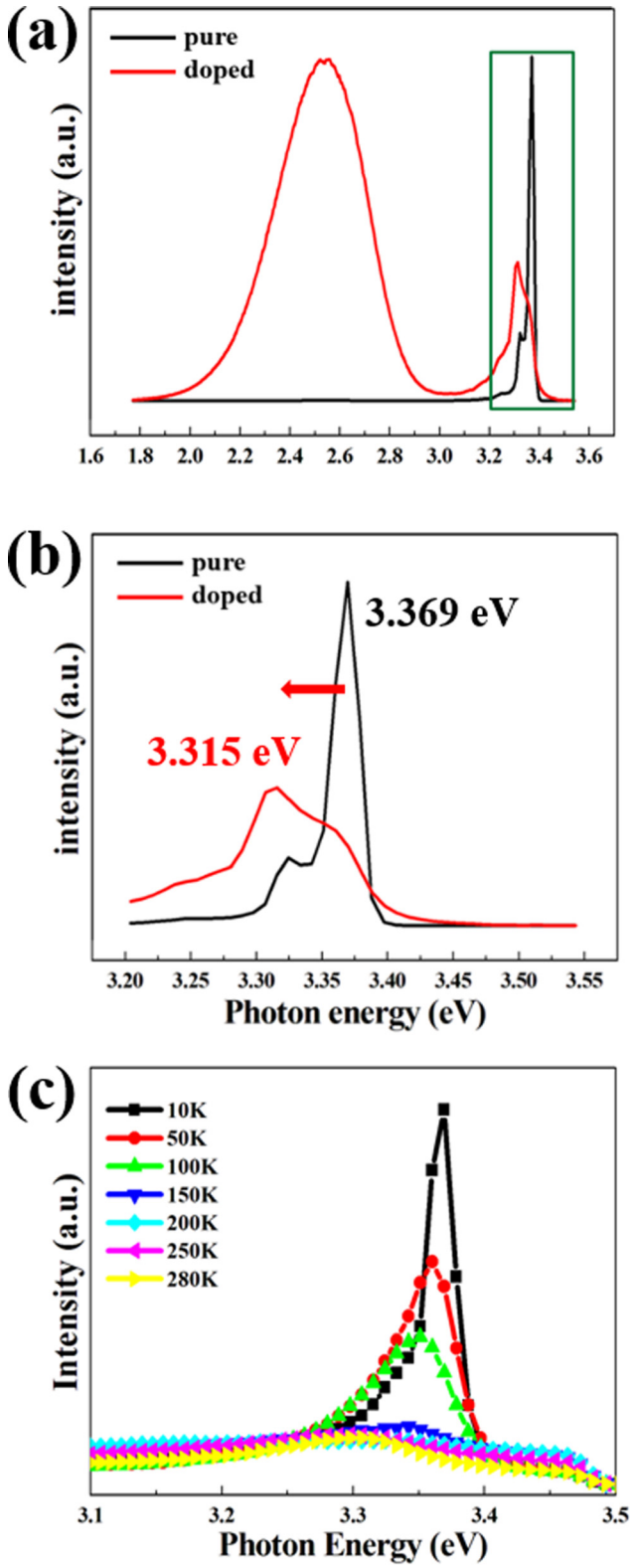

FIG. 3. (a) The PL spectra of Sb-doped ZnO NWs and pure ZnO NWs. (b) Spectra highlighted in (a). (c) PL spectra of Sb-doped ZnO NWs at various temperatures.

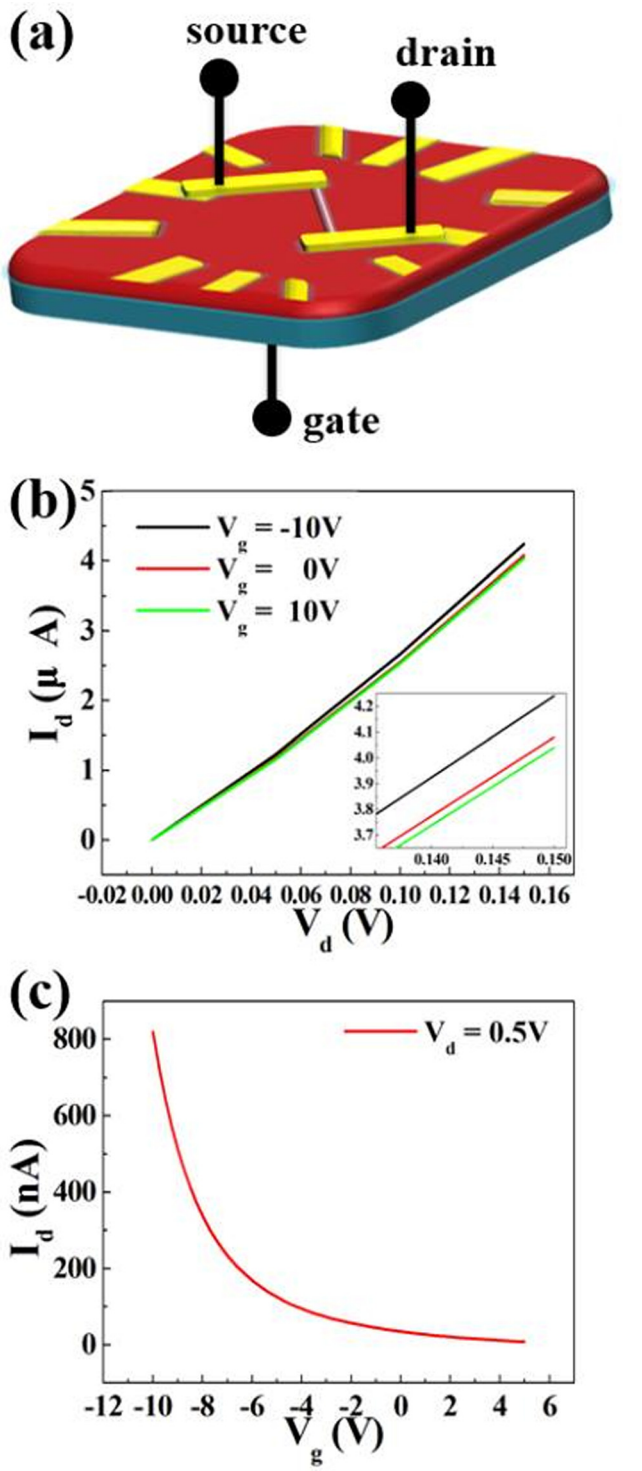

FIG. 4. (a) The schematic diagram of the NWFET device. (b) The I_d vs V_d curve at different V_g. The inset shows the I_d vs V_d curve when $V_d > 0.135$ V. (c) I_d vs V_g at $V_d = 0.5$ V.

V_g at a constant V_d of 0.5 V. The inset highlighted the I_d vs V_d curve ($V_d > 0.135$ V). The device of the FET process in Figs. 4(b) and 4(c) is not the same device. The original device was damaged due to other testing for other purposes. We have fabricated another devices and tested the electrical properties all over again, and the result has shown good reproducibility. This is even better because it provides more evidence of p-type conduction in the Sb-doped ZnO NW. The gating effect would be a bit different because of inevitable differences between devices. The NW-FET characterization shows that I_d increases at negative V_g, indicating that the Sb-doped ZnO NWs exhibit p-type conductivity. The role of Sb in Sb-doped ZnO NWs is that Sb replaced Zn accompanying two Zn vacancies ($Sb_{Zn} - 2V_{Zn}$), which regards as acceptors lead to p-type conduction. The doped

Sb within single ZnO NWs are confirmed by TEM Energy Dispersive Spectrum (EDS) mapping (Fig. 2(a)), and the p-type properties are measured by FET device (Fig. 4). The carrier mobility can be estimated by using the following equations:[35,36]

$$\mu = \frac{L^2}{CV_d}\left(\frac{dI_d}{dV_g}\right), \tag{1}$$

$$C = \frac{2\pi\varepsilon_0\varepsilon_{SiO_2}L}{\ln\left(\frac{4h}{d}\right)}, \tag{2}$$

where μ is the carrier mobility, L is the channel length of the NW, C is the capacitance, ε_{SiO2} is the dielectric constant of SiO_2 (3.9), h is the thickness of dielectric layer, and d is the diameter of the NW, respectively. From Eqs. (1) and (2), the mobility is calculated to be 21.610 $cm^2\ V^{-1}\ s^{-1}$. Moreover, the hole concentration can be estimated by using the equation as follows:

$$n_h = \frac{V_{th}C}{q\pi\left(\frac{d}{2}\right)^2 L}, \tag{3}$$

where V_{th} is the threshold voltage. The hole concentration is then calculated to be about $5.767 \times 10^{17}\ cm^{-3}$.

Fig. 5(a) shows the IV curve of single Sb-doped ZnO NW, and the inset is the corresponding FESEM image of the device. The I-V curve is linear, suggesting that the contact electrode is ohmic. The resistivity of the NW can be estimated by the following equation:

$$\rho = R\frac{A}{L}, \tag{4}$$

where ρ is the resistivity, R is the resistance, and A is the cross-section area of the wire. The resistivity is calculated to be $1.727 \times 10^{-2}\ \Omega$ cm, which is favorably compatible to that of pure ZnO NWs by $1 \sim 2$ orders lowered. The 254 nm UV illumination was used as the excitation source for the Sb-doped ZnO NW photodetector at a bias of 0.5 V. The schematic diagram and photoresponse of the device are shown in Figs. 5(b) and 5(c), respectively. The dark current is about 10.3 μA. When the UV light is on, the depletion zone is thinner in contrast to that of UV-off state.[18] As the UV light turned off, the oxygen vacancies will generate O^- and OH^- ions in the surface of the nanowires, resulting in a thick depletion zone. On the other hand, when UV light turned on, the electron-hole pairs were generated. The holes would recombine the surface ions of O^- and OH^- to release in gas, resulting in the free carriers for conductive band and make the depletion zone thinner. Thus, the conductivity is enhanced and the photocurrent is about 11.6 μA. Once the UV light is off, the current drops and the conductivity is decreased. Once again, it may be attributed to the depletion region recovery back to original state.

In summary, we have synthesized Sb-doped ZnO NWs on Si (100) substrates by thermal evaporation method and VLS mechanism. HRTEM demonstrated the Sb-doped ZnO NWs single crystalline of wurtzite structure with [1-1-2] growth direction. The XPS spectra have shown that the Sb-doped ZnO NWs exhibited Sb-3d[3] peak at 539.9 eV and indicated the Sb concentration in ZnO NWs was about 2.49 at. %. Furthermore, a red shift of the PL spectra occurred for the Sb-doped ZnO NWs in contrast to that of ZnO NWs. It may be attributed that doping with Sb into ZnO NWs causes the reduction of band gap by band-tailing. Electrical transport properties of single NWFETs exhibited the p-type semiconductor characterization. High carrier mobility of 21.610 $cm^2\ V^{-1}\ s^{-1}$ and carrier concentration of $5.767 \times 10^{17}\ cm^{-3}$ were achieved. In addition, we have shown the potential application of Sb-doped ZnO NWs for UV photodetector. The current rise/drop is obviously dependent on light on/off, respectively. These properties make the Sb-doped p-type

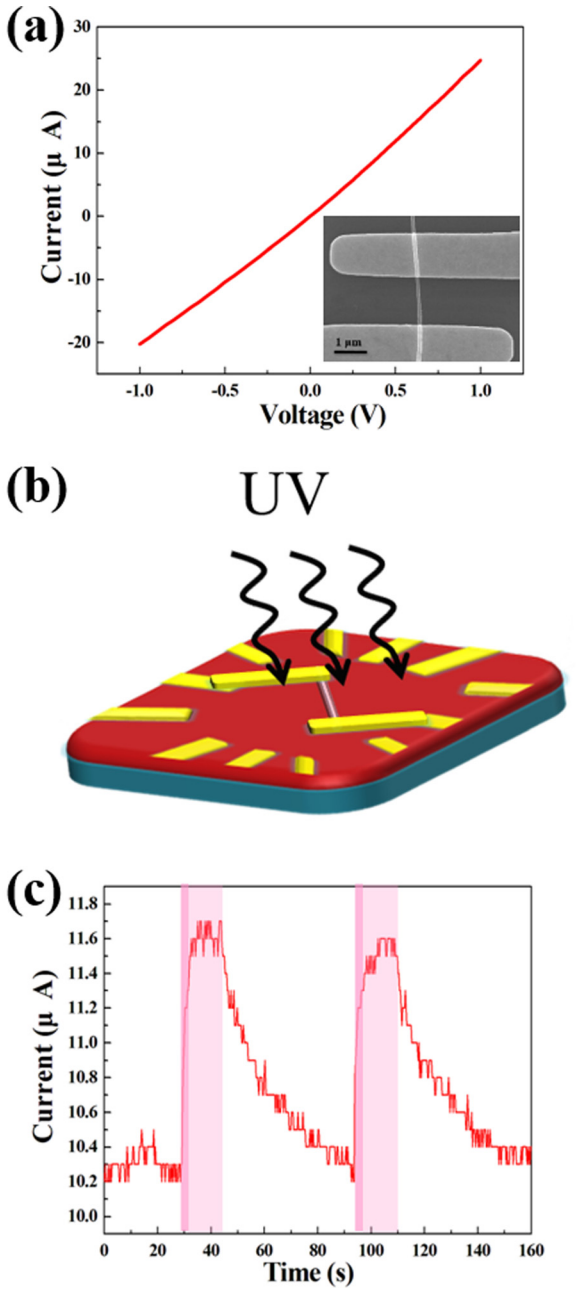

FIG. 5. (a) The I-V curve of the single Sb-doped ZnO NW. The inset shows the corresponding FESEM image of the device. (b) The schematic diagram of Sb-doped ZnO NWs photodetector. (c) The photoresponse of the device with 254 nm UV light illumination.

ZnO NWs a promising candidate for electronic and optoelectronic devices in the future.

The authors would like to acknowledge the support by the National Science Council through Grant Nos. NSC 100-2628-E-009-023-MY3 and NSC 102-2221-E-009-039.

[1]Z. L. Wang, Mater. Today **7**(6), 26 (2004).
[2]Y. Li, F. Della Valle, M. Simonnet, I. Yamada, and J.-J. Delaunay, Nanotechnology **20**(4), 045501 (2009).
[3]S. Bai, W. Wu, Y. Qin, N. Cui, D. J. Bayerl, and X. Wang, Adv. Funct. Mater. **21**(23), 4464 (2011).
[4]C.-Y. Kao, C.-L. Hsin, C.-W. Huang, S.-Y. Yu, C.-W. Wang, P.-H. Yeh, and W.-W. Wu, Nanoscale **4**(5), 1476 (2012).
[5]M. Law, L. E. Greene, J. C. Johnson, R. Saykally, and P. Yang, Nature Mater. **4**(6), 455 (2005).
[6]W.-K. Hong, J. I. Sohn, D.-K. Hwang, S.-S. Kwon, G. Jo, S. Song, S.-M. Kim, H.-J. Ko, S.-J. Park, M. E. Welland, and T. Lee, Nano Lett. **8**(3), 950 (2008).
[7]W. I. Park and G. C. Yi, Adv. Mater. **16**(1), 87 (2004).
[8]M.-T. Chen, M.-P. Lu, Y.-J. Wu, J. Song, C.-Y. Lee, M.-Y. Lu, Y.-C. Chang, L.-J. Chou, Z. L. Wang, and L.-J. Chen, Nano Lett. **10**(11), 4387 (2010).
[9]Z. L. Wang and J. Song, Science **312**(5771), 242 (2006).
[10]Y. Yang, K. C. Pradel, Q. Jing, J. Ming Wu, F. Zhang, Y. Zhou, Y. Zhang, and Z. L. Wang, ACS Nano **6**(8), 6984 (2012).
[11]V. Bhosle, A. Tiwari, and J. Narayan, J. Appl. Phys. **100**(3), 033713 (2006).
[12]H. Wei, Y. Wu, L. Wu, and C. Hu, Mater. Lett. **59**(2–3), 271 (2005).
[13]T.-H. Fang and S.-H. Kang, Curr. Appl. Phys. **10**(4), 1076 (2010).
[14]S. Y. Bae, C. W. Na, J. H. Kang, and J. Park, J. Phys. Chem. B **109**(7), 2526 (2005).
[15]V. Vaithianathan, J. H. Moon, C.-H. Chang, K. Asokan, and S. S. Kim, J. Nanosci. Nanotechnol. **6**(11), 3422 (2006).
[16]V. Vaithianathan, B.-T. Lee, and S. S. Kim, Appl. Phys. Lett. **86**(6), 062101 (2005).
[17]G. Wang, S. Chu, N. Zhan, Y. Lin, L. Chernyak, and J. Liu, Appl. Phys. Lett. **98**(4), 041107 (2011).
[18]J. M. Wu, C.-W. Fang, L.-T. Lee, H.-H. Yeh, Y.-H. Lin, P.-H. Yeh, L.-N. Tsai, and L.-J. Lin, J. Electrochem. Soc. **158**(1), K6 (2011).
[19]U. Wahl, J. G. Correia, T. Mendonça, and S. Decoster, Appl. Phys. Lett. **94**(26), 261901 (2009).
[20]F. Wang, J.-H. Seo, D. Bayerl, J. Shi, H. Mi, Z. Ma, D. Zhao, Y. Shuai, W. Zhou, and X. Wang, Nanotechnology **22**(22), 225602 (2011).
[21]Y. Yang, J. Qi, W. Guo, Q. Liao, and Y. Zhang, CrystEngComm **12**(7), 2005 (2010).
[22]S. H. Kim, A. Umar, Y. K. Park, J. H. Kim, E. W. Lee, and Y. B. Hahn, J. Alloys Compd. **479**(1–2), 290 (2009).
[23]A. B. Yankovich, B. Puchala, F. Wang, J.-H. Seo, D. Morgan, X. Wang, Z. Ma, A. V. Kvit, and P. M. Voyles, Nano Lett. **12**(3), 1311 (2012).
[24]I. A. Palani, D. Nakamura, K. Okazaki, M. Higashihata, and T. Okada, Mater. Sci. Eng., B **176**(18), 1526 (2011).
[25]J.-W. Kang, Y.-S. Choi, M. Choe, N.-Y. Kim, T. Lee, B.-J. Kim, C. W. Tu, and S.-J. Park, Nanotechnology **23**(49), 495712 (2012).
[26]I. A. Palani, K. Okazaki, D. Nakamura, K. Sakai, M. Higashihata, and T. Okada, Appl. Surf. Sci. **258**(8), 3611 (2012).
[27]W. E. Mahmoud, F. Al-Marzouki, S. Al-Ameer, and F. Al-Hazmi, J. Appl. Crystallogr. **45**(2), 182 (2012).
[28]Y. Yang, W. Guo, J. Qi, J. Zhao, and Y. Zhang, Appl. Phys. Lett. **97**(22), 223113 (2010).
[29]A. B. Djurišić, A. M. C. Ng, and X. Y. Chen, Prog. Quantum Electron. **34**(4), 191 (2010).
[30]Y. Yang, J. Qi, Q. Liao, Y. Zhang, L. Tang, and Z. Qin, J. Phys. Chem. C **112**(46), 17916 (2008).
[31]J.-M. Wu, J. Phys. Chem. C **112**(34), 13192 (2008).
[32]X. Fang, J. Li, D. Zhao, B. Li, Z. Zhang, D. Shen, X. Wang, and Z. Wei, Thin Solid Films **518**(20), 5687 (2010).
[33]Q. Li, K. Gao, Z. Hu, W. Yu, N. Xu, J. Sun, and J. Wu, J. Phys. Chem. C **116**(3), 2330 (2012).
[34]K. H. Tam, C. K. Cheung, Y. H. Leung, A. B. Djurišić, C. C. Ling, C. D. Beling, S. Fung, W. M. Kwok, W. K. Chan, D. L. Phillips, L. Ding, and W. K. Ge, J. Phys. Chem. B **110**(42), 20865 (2006).
[35]R. Tu, L. Zhang, Y. Nishi, and H. Dai, Nano Lett. **7**(6), 1561 (2007).
[36]J. Goldberger, D. J. Sirbuly, M. Law, and P. Yang, J. Phys. Chem. B **109**(1), 9 (2005).
[37]See supplementary material at http://dx.doi.org/10.1063/1.4869355 for the compare of growth parameters and the schematic diagram of electrical sample fabrication process.